The Study of Carbon Nanotubes as electrode materials and Metal Coordination Complexes as Molecular Spacers to be Used in Supercapacitors' Applications

by

Nesreen Elathram

A thesis submitted to the faculty of
The University of North Carolina at Charlotte
in partial fulfillment of the requirements
for the degree of Bachelors of Science with
Honors

Charlotte

Spring 2018

Approved by:

Dr. Jordan C. Poler

Dr. Brian Cooper

Dr. Jon Merkert

ABSTRACT

Supercapacitors with higher energy density, faster power capability, and longer cycle life are needed to effectively store electrical energy. Carbon nanotubes (CNTs) are used as supercapacitor materials due to their significant specific surface area (SSA). Altering the surface of nanotubes by adsorbing different spacers, can have an effect on their functionality and make them more applicable for future supercapacitors for energy storage applications. This thesis describes the dispersion stability of CNTs that are variant in the size and chirality, and investigates various dinuclear molecular coordination complexes that showed adsorption on CNTs surfaces. Moreover, since zinc and copper are an earth abundant metals, these complexes can be used as components in sustainable energy storage materials. Modeling of the adsorption isotherm is best fit with the BET and Langmuir models and membrane resistance data are consistent with the complexes acting as molecular spacers between the SWCNTs in a condensed thin film.

DEDICATION

To my beloved family and to my wounded home

ACKNOWLEDMENTS

Thanks to the merciful lord for all the countless gifts he has given me

I would like to thank Dr. Jordan Poler for everything he has done and taught. He was my biggest supporter in my undergraduate study at UNC Charlotte. It is a great honor to work under his supervision. He has inspired me and had the most profound impact on me with his rich attitudes on science and beyond. I would also like to thank my incredible group members for all the help and support. I spent large amount of time with them and learn and exchange knowledge with. I finally would like to express my gratitude to the honors college advisor Dr. Daniel Jones and my honors thesis committee members Dr. Jon Merkert and Dr. Brain Cooper for the endless help and generous advice and also to the department of chemistry at UNC Charlotte for striving to create the best environment for research and creativity.

TABLE OF CONTENTS

ABSTRACT 2

DEDICATION 3

ACKNOWLEDMENTS 4

CHAPTER 1: INTRODUCTION 7

CHAPTER 2: EXPERIMENTAL 15

2.1 Making Dispersion and Spacer Solutions 15

2.2 Dispersion Stability Measurements 15

2.3 Adsorption Isotherm Measurements 16

2.4 Zeta Potential and Size Measurements 16

2.5 UV-Vis NIR Spectroscopy 16

2.6 Membrane Resistance Measurements 17

CHAPTER 3: RESULTS AND DISCUSSION 18

3.1 Dispersion Stability Measurements 18

3.2 Adsorption Studies 30

3.3 Zeta Potential and Size Measurements 34

3.4 UV-Vis NIR Spectroscopy 35

3.5 Membrane Resistance Measurements 39

CHAPTER 4: CONCLUSIONS AND FUTURE WORK 43

BIBLIOGRAPHY 45

CHAPTER 1: INTRODUCTION

Due to the environmental contamination caused by burning of fossil fuels, the world is shifting to alternative energy sources, such as solar, tidal, and wind energy, which have lower carbon emissions and do not have harmful consequences.[1] However, fossil fuels represent the major source of energy consumed in the U.S., while the energy provided by alternative energy sources represents around 10% of the consumption (Fig. 1), and this can be attributed to the deficiency in efficient technical ways to store energy extracted from clean resources. Therefore, this energy needs to be stored to ensure the presence of an energy supply when the sun sets, and when there is no wind.

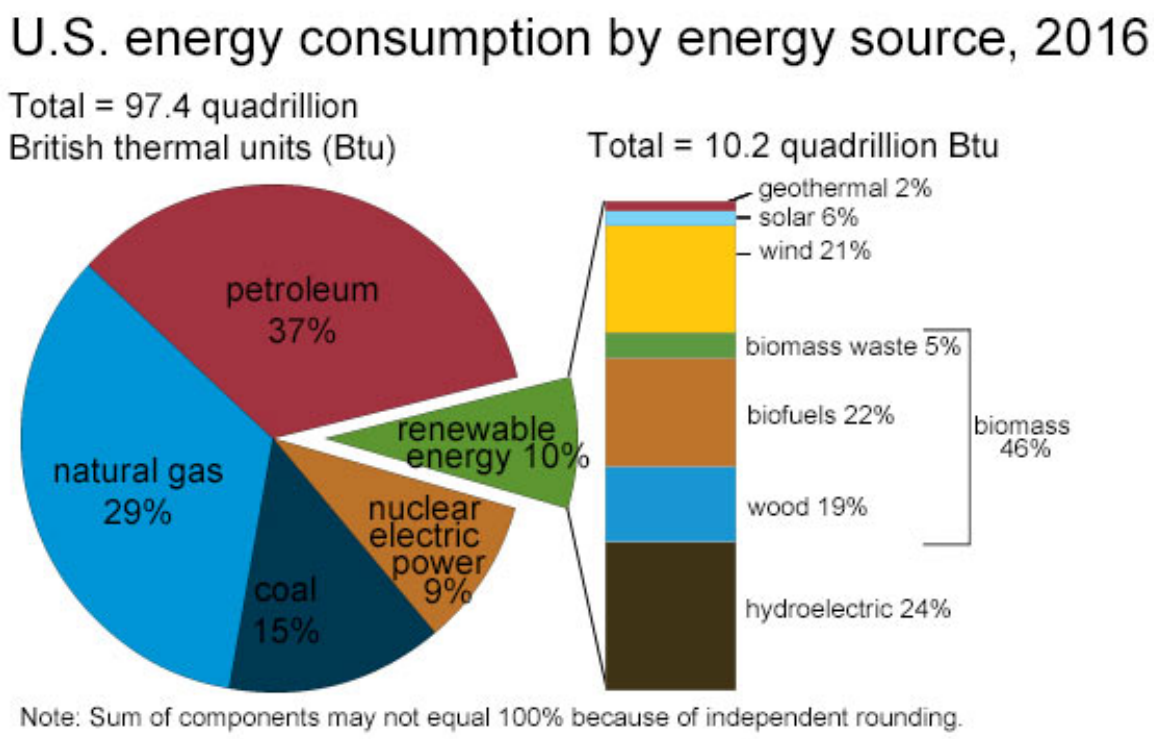

Figure 1: U.S. energy consumption of 2016.[2] fossil fuel represents the major source of energy consumed in the United States while the energy obtained from clean resources repents small fraction of the consumption.

Batteries and capacitors are the common devices used to store electrical energy. Batteries have high energy density, low power density and shorter life cycles; they can function for hundreds of charge-discharge cycles; however, capacitors have a low energy density, high power density and longer life cycles. They can function for hundreds of thousands of cycles (Fig. 2). The energy storage can be improved by either improving the energy density of the capacitors or increasing the power density of batteries. The energy density of the capacitors can be improved by developing new electrochemical supercapacitors. Capacitors can take two forms: electrical double-layer capacitors (EDL) and pseudo capacitors, that store the electrical charge faradaically through transfer electron charge between electrode and electrolyte. Conventional double-layer capacitors store energy electrostatically through two separated electrode layers (electrical double-layer capacitance mechanism). The energy stored in the capacitor increases with the surface area of the separated electrodes. Since energy storage is directly proportional to the surface area of the capacitor layers, electrode material can be made from a substance has a higher surface area; therefore, more energy can be stored, making these materials promising for supercapacitors for future energy storage.[3]

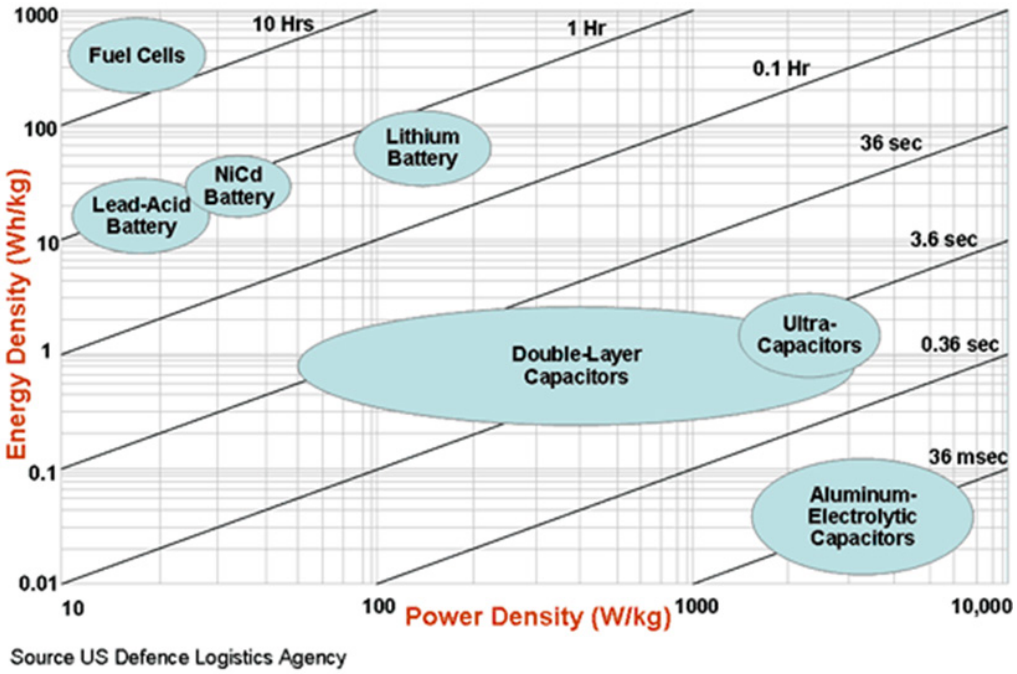

Figure 2: Ragone plot, comparison between energy and power densities of different energy storage devices.[4]

Nanoscale materials have smaller volumes and higher specific surface areas than bulk materials. In both energy storing devices (electrical double-layer capacitors and pseudo capacitors), carbon nanotubes (CNTs) can be used as building materials of these capacitors; they have high electrical conductivity and high specific surface area (SSA) on which charges can be stored, making them viable materials in the production of these supercapacitors. Moreover, altering the surface of nanotubes and adding spacers could have a great impact on their functionality and make them good solutions for many environmental technical problems.

Pseudo capacitor or redox capacitance uses fast redox reactions as an energy storage technique making them better capacitors than EDL capacitors. Oxides of transition metals oxides were studied as electrode material for these pseudo capacitors such as MnO_2 [5]. Manganese is a transition metal that can have multiple oxidation states and a high capacitance; however, it shows

low electronic conductivity and poor conformational stability, therefore, conductive metals such as Ni were implanted in MnO_2 nanoflowers, and XRD, EDS and SEM were used to analyze the material. Another method used MnO_2 in combination with TiN; MnO_2 was adsorbed onto TiN, making nanotube hybrids with higher functional electrode, and, therefore, capacitance.[6] Since nanostructured carbon materials showed good stability as a supercapacitor candidate and TiO_2-B nanomaterials provided high power densities as material for lithium-ion batteries, hybrid supercapacitors with a CNTs cathode and TiO_2-B nanowire anode showed higher energy storage, small resistivity and high-power density.[7]

This research studies carbon nanotubes CNTs as potential electrode materials in electrical double-layer supercapacitor due to their high SSA and electrical conductivity. However, CNTs tend to aggregate when dispersed at high concentration and reduce their SSA, making them less efficient as basic materials for many scientific applications. To prevent the self-assembly of CNTs and to increase the electron transfer and ion adsorption onto their surface and, therefore, increase the energy storage capabilities of these nanostructured carbon materials, molecular spacers were added (Fig. 3). Two different types of compounds —mononuclear complexes and multinuclear complexes — were used as molecular spacers in CNTs dispersions. Long range interactions (LRI) between those ionic species and CNTs were studied.[8] Dispersion stability and aggregation kinetics were conducted to the tubes with all the spacers, and because metal complexes can transfer charges with carbon nanotubes, they work as better spacers in CNTs dispersions than inorganic salts that do not bind strongly to the tubes.[8] Furthermore, solvents might affect the stability of CNTs and how these tubes interact with the spacer. Two common dispersing non-aqueous solvents were studied, *N,N*-dimethylformamide (DMF) and *N*-methyl-2-

pyrrolidinone (NMP). Different mixtures of the solvents were examined and the dispersion stability of CNTs was measured and showed high stability in mixtures of both DMF and NMP.[9]

Metal coordination complexes were adsorbed to single-walled carbon nanotubes as potential molecular spacers: dinuclear ruthenium coordination complex +2Ru2 (Fig. 5), dinuclear zinc coordination complex +2Zn2 (Fig. 4), copper ferrocenoyl coordination complexes +2Cu2FcOH and Cu2FcOH (Figs. 6 and 7), [10] When molecular spacers intercalate between SWCNTs, they work as a barrier between tubes preventing their aggregation and increasing the ion-accessible SSA, making them good materials for supercapacitors. Dispersion stability measurements were conducted to determine the stability of CNTs in DMF using the +2Zn2 hydrazone, +2Ru2 and Cu2FcOH complexes.

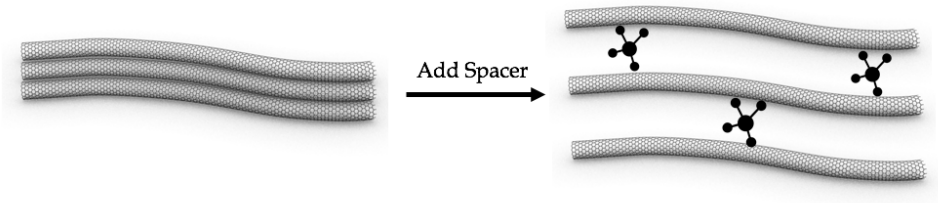

Figure 3: the spacers intercalation between the CNTs

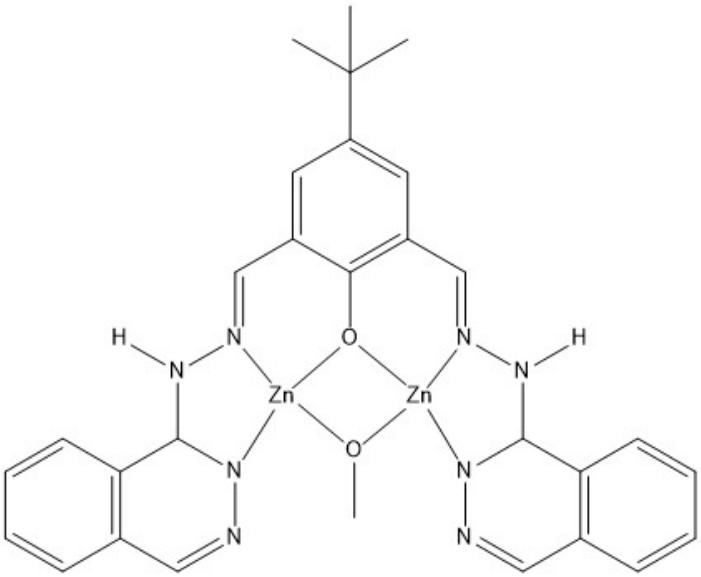

Figure 4: The molecular structure of zinc hydrazone coordination complexes, 4-(tert-butyl)-2,6-bis((2-(phthalazin-1-yl)hydrazono)methyl)phenol (m2-methoxo) dizinc(II).**(+2Zn2)**[9]

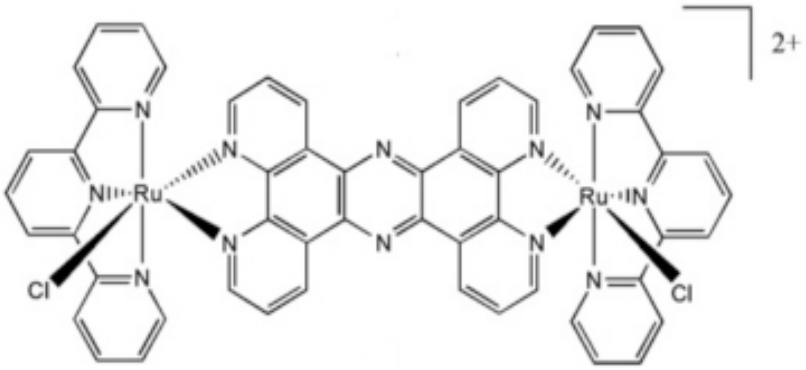

Figure 5: The molecular structure of Ruthenium coordination complex, Cl(2,2' ;6' ,2''-terpyridine)Ru(tetrapyrido- [3,2-α:2' ,3' -*c*:3'',2''-*h*:2'',3''-*j*]phenazine)Ru(2,2' ;6' ,2''-terpyridine)Cl]- $(PF_6)_2$ **(+2Ru2)**

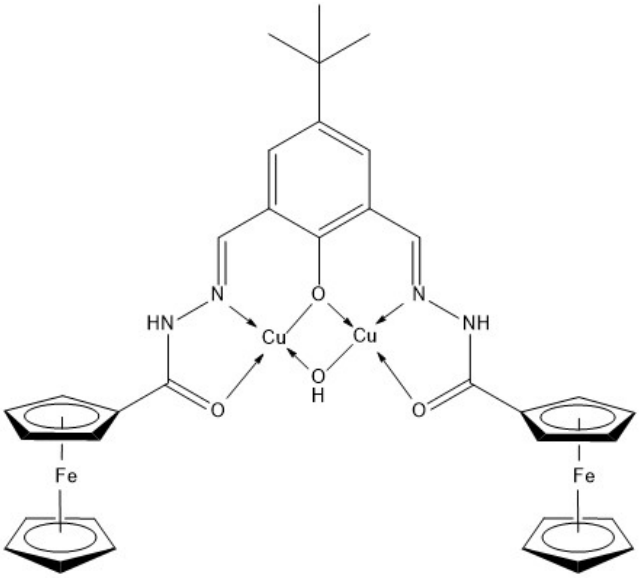

Figure 6: Copper ferrocenoylhydrazone hydroxide *biscopper [4-tert-butyl-2,6-diformylphenol bis-ferrocenoylhydrazone hydroxide]* **(Cu2FcOH)**

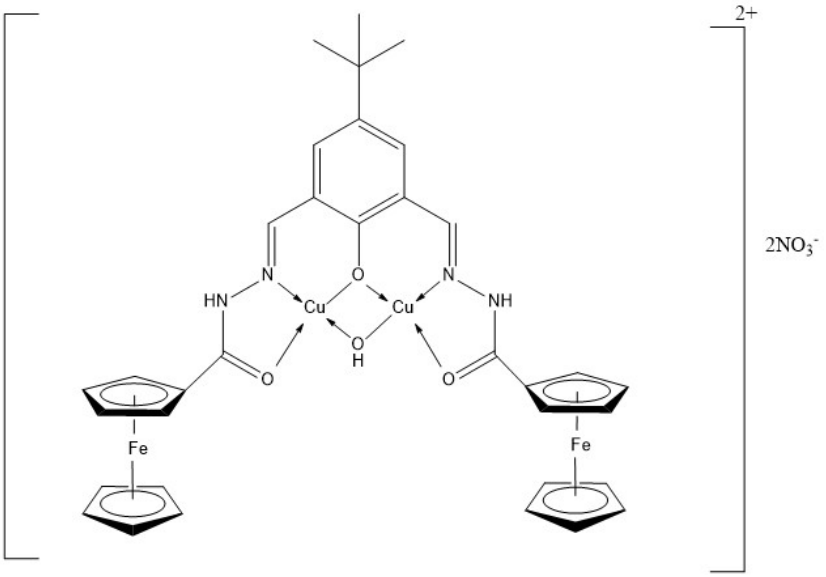

Figure 7: Copper ferrocenoylhydrazone hydroxide *biscopper [4-tert-butyl-2,6-diformylphenol bis-ferrocenoylhydrazone hydroxide]* **(+2Cu2FcOH)**

The coagulants were added into the SWCNT dispersion. The metal complexes have different charges and nuclearity. The complexes are expected to experience π-π stacking interactions with the SWCNTs due to the π electrons in their ligands. By adsorbing coordination complex molecules to the surface of CNTs, they prevent the their self-assembly by working as spacer to prevent the aggregation and also to increase the increase charge storage and guarantee higher loading of electroactive material and therefore increasing the capacitance. The adsorption of coordination complex data is understood by LRI between the tubes and the molecular spacers such as electrostatic interactions between charged particles, π-π stacking interactions and van der Waals forces. A full characterization of the molecular spacers was conducted to access potential application in energy storage devices. A fundamental understanding of how molecular spacers interact with CNTs will be discussed.

CHAPTER 2: EXPERIMENTAL

2.1 Making Dispersion and Spacer Solutions

Carbon nanotubes dispersion was made by adding CNTs (0.5 mg) in N,N-dimethlyformamide (30 mL) in 40 mL vial and tip ultrasonicated it at 10 W RMS for 25 min. Then ultra-centrifuged at 20,000 g for 20 min, to remove the aggregated tubes. The supernatant was collected as the dispersion. Sodium bromide, NaBr, was used as purchased and was dried in a vacuum oven overnight. The molecular coordination complexes were used as synthesized and were dried in a vacuum oven. Stock solutions of NaBr, dinuclear copper coordination complex, biscopper [4-*tert*-butyl-2,6-diformylphenol bis-ferrocenoylhydrazone chloride] (Cu_2F_cOH), dinuclear zinc coordination complex 4-(*tert*-butyl)-2,6-bis((2-(phthalazin-1-yl)hydrazono)methyl)phenol (m_2-methoxo) dizinc(II)-acetate (+2Zn2) and ruthenium coordination complex, [Cl(2,2' ;6' ,2''-terpyridine)Ru(tetrapyrido- [3,2-α:2' ,3' -*c*:3'',2''-*h*:2'',3''-*j*]phenazine)Ru(2,2' ;6' ,2''-terpyridine)Cl]- $(PF_6)_2$ (+2Ru2) [9] were made by dissolving the spacer in DMF , (2.1 mg -18.6 mg) in DMF 7 mL.

2.2 Dispersion Stability Measurements

Molecular spacers were adsorbed on the surface of CNTs by adding different concentrations (0 μM – 1200 μM) of coagulants and left to incubate for 48 h. They were ultra-centrifuged at 10000 g for 10 min to remove the aggregated tubes. Using Cary 5000 UV-Vis-NIR spectrometer, the concentration of remaining CNTs in the supernatant were measured at absorption wavelength of each CNT being studied and normalized to the control pristine dispersion. the control sample contains CNTs dispersion without adding any spacer.

2.3 Adsorption Isotherm Measurements

Molecular spacers were adsorbed on the surface of CNTs by adding different concentrations of coagulants and left to incubate for 2 h. They were filtered through polypropylene membranes (0.2 Micron, 13mm 100/Pk). Using a Cary 5000 UV-Vis-NIR spectrometer, the concentrations of remaining spacers in the DMF solution were measured according Beer's law.

2.4 Zeta Potential and size measurements

Malvern instrument and Zetasizer software, zeta Potential measurements were conducted on a dilute dispersion of few-walled carbon nanotubes (FWCNTs) and compared to the other Zeta Potential values obtained for single walled CNTs of chirality 6,5 (Signis® SG65), single walled CNTs of chirality 7,6 (Signis® SG76) and High-pressure carbon monoxide (HiPCo) tubes.

2.5 UV-Vis NIR spectroscopy

A Cary 5000 UV-Vis-NIR spectrometer was used to measure absorbance spectra of +2Zn2, +2Ru2 and Cu2FcCl molecular spacers in DMF. UV-Vis absorption was recorded from 300-800 nm with spectral bandwidth of 1.0 nm. Quartz cuvettes with path width of 1 cm were used.

2.6 Membrane resistance measurements

1-Successive DMF Rinses Method

Wet Pristine Films:

Membrane resistance measurements were made using vacuum filtration across a 9.55×10^{-4} m^2 0.272 mg thin film of SWCNTs. The flow rate of DMF through the membrane was measured for successive 50.0 mL rinses. The film was formed onto a 0.45 µm pore polypropylene membrane and the flow time and the pressure difference were measured.

Dry Pristine Films:

The same procedure was conducted to pristine films after they have been vacuum dried for different times to compare and find out if the amount of the DMF stuck in the film affects the permeability of the film and slows it down. One of the films was vacuum dried for one hour, another one overnight and the last for two days.

+2Zn2-SWCNTs Thin Films:

Thin films of CNTs with coagulant (0.262 mg) were made by vacuum filtering the CNTs with spacer dispersion on polypropylene films (9.55 10^{-4} m^2 and 0.45 mm). the coagulant was added to dispersion and left to incubate for 90 min. Successive rinses of DMF (50 mL) were pushed through the film to measure the change in flux of DMF. Membrane resistance measurements were performed to pristine CNTs and CNTs-coagulant dispersions. To determine the flux Q, the filtrate were measured after each rinse.

CHAPTER 3: RESULTS AND DISCUSSION

3.1 Dispersion Stability Measurements

In previous work, it has been shown that the presence of multinuclear spacers affects the stability of the tube-tube repulsive barrier [8]. Changing the nuclearity, the charge, and concentration of the spacers controls the onset of aggregation. We measured the dispersion stability (X_o) which is the concentration of the coagulant at which half of the dispersed tubes aggregated.[8]

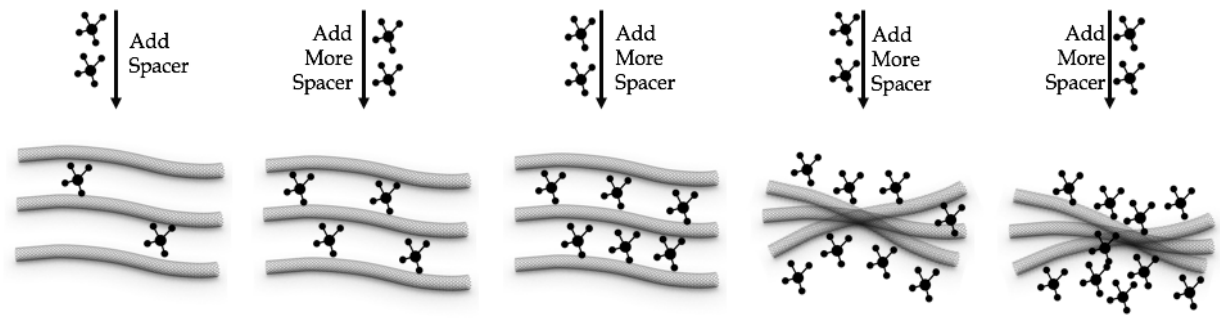

Figure 3.1.1: Dispersion stability measurements.

Dispersion stability measurements were conducted in order to determine the stability of CNTs in DMF after different concentrations of +2Zn2 hydrazone, +2Ru2 and Cu2FcOH ferrocenoylhydrazone complexes were added into the CNT dispersion (Fig. 3.1.1). The concentration of CNTs was measured as the ionic strength was increasing. Five different size and chirality carbon nanotubes were used: three SWCNTs one, double-walled CNTs and one, MWCNT. Due to the difference in tube diameter between different CNTs, dispersion stability measurements were conducted to determine the differences in their stabilities in DMF once the +2Zn2 hydrazone complex was added into the SWCNT dispersion. Since the +2Zn2 hydrazone

is positively charged and the surface of the SWCNTs have a partial negative charge due to delocalized π electrons, the two materials will interact electrostatically, which effectively collapses the electrical-double layer of individual SWCNTs. Once the +2Zn2 hydrazone collapses the electrical-double layer of the tubes, the tubes can aggregate together, forming bundles of tubes, which are easily removed by centrifugation.

The dispersion stability of +2Zn2 in HiPCO tubes was X_o = 14.2 ± 0.3 μM, in SG 6,5 tubes was X_o = 32.9 ± 0.4 μM, in SG 7,6 tubes was 22.7 ± 0.3 and X_o = 35 ± 6 μM for FWCNT (Table 1). It was hypothesized that +2Zn2 binds more strongly to the larger tubes because there is less strain on the complex to bind around the surface of the tube, i. e., +2Zn2 binds more strongly to the larger HiPco (7,7) tubes causing the EDL to collapse and that forces the system to aggregate, which drastically reduces the SSA, making the tubes less effective in energy storage application. Smaller tubes have higher dispersion stability than larger ones.

The dispersion stability of +2Ru2 in HiPco tubes was X_o = 1.37 ± 0.02 μM and in SG 6,5 tubes was X_o = 1.35 ± 0.02 μM which shows insignificant difference in the stability between different size tubes and that can be attributed to the very strong binding of +2Ru2 to tubes leading to faster aggregation. The dispersion stability of HiPco SWCNTs in +2Zn2 is larger than that measured for the +2Ru2 species, 1.37 ± 0.02 μM (Fig. 3.1.7). Both of the complexes should have the same charge and similar π-π stacking interactions with the SWCNTs, but the +2Zn2 acetate salt does not dissociate completely in DMF, which reduces the ionic strength at the dispersion, and therefore does not collapse the electrical double layer. This leads to significantly higher loading of the electroactive complexes onto the SWCNTs, which may increase their utility as supercapacitor materials.

CNTs dispersion have low dispersion stability limit with +2Ru2 compared to other spacers due to stronger binding to the surface of the tubes. Although +2Ru2 spacer binds more strongly, the loading of the spacer onto SWCNT is much lower than with the other spacers. Unlike +2Zn2 hydrazone, Cu2FcOH spacer has no charge and therefore, it does not dissociate in DMF, which reduces the ionic strength, and therefore does not collapse the electrical double layer. This leads to significantly higher loading of the electroactive complexes onto the SWCNTs, which may increase their utility as supercapacitor materials. The dispersion stability of CNTs in Cu2FcOH is much higher than with +2Zn2 hydrazone because the Cu2FcOH complex spacer does not have a charge, which reduces the ionic strength, and therefore does not collapse the electrical double layer. As a result, Cu2Fc complex is better in dispersing CNTs than +2Zn2 hydrazone. However, The +2Zn2 complex binds stronger than Cu2FcOH to the CNTs due to electrostatics and π-π stacking interactions, but decrease CNT stability due to a more rapid collapse of the electric double layer (EDL).

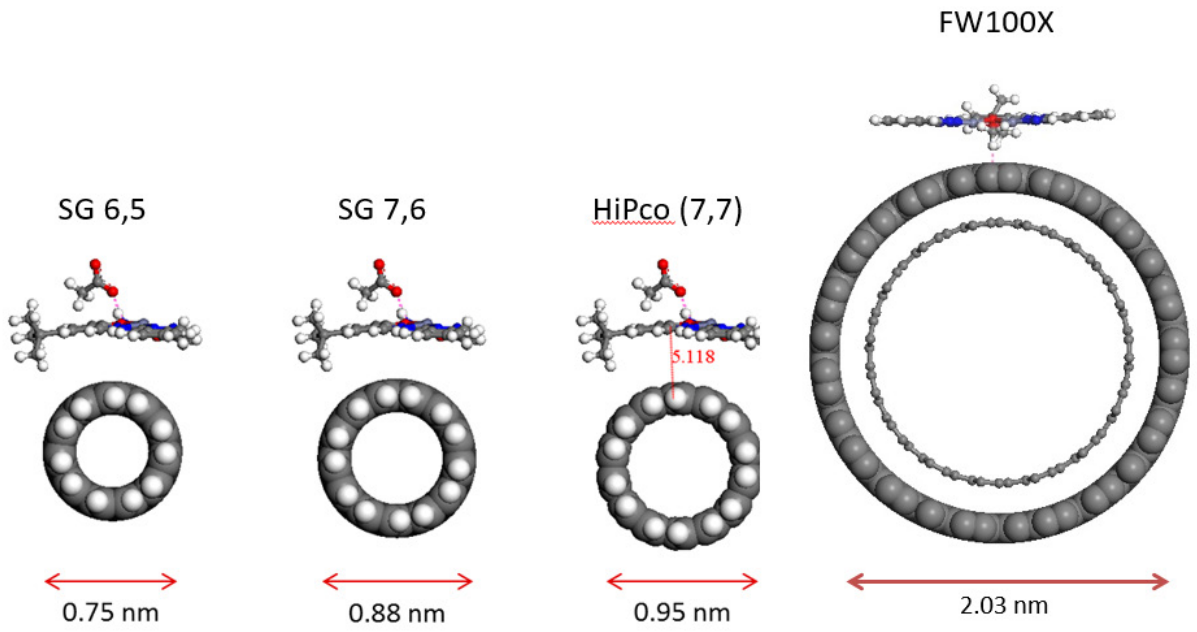

Figure 3.1.2: The Molecular model of different size and chirality CNTs intercalated by +2Zn2 hydrazone acetate salt. From left to right, the diameter of the SWCNT increases as it models SG 6,5 SWCNTs; SG 7,6 SWCNTs; and HiPCO SWCNTs (SG 7,7), respectively.

CNTs	**Diameter (nm)**	**X_0 (μM)**
SG 6,5	0.75	32.9 ± 0.4
SG 7,6	0.88	22.7 ± 0.3
HiPco	0.95	14.2 ± 0.3
FW100X	2.03	35 ± 6

Table 3.1.1: Dispersion stabilities CNTs in +2Zn2 coordination complex with their corresponding tube diameters.

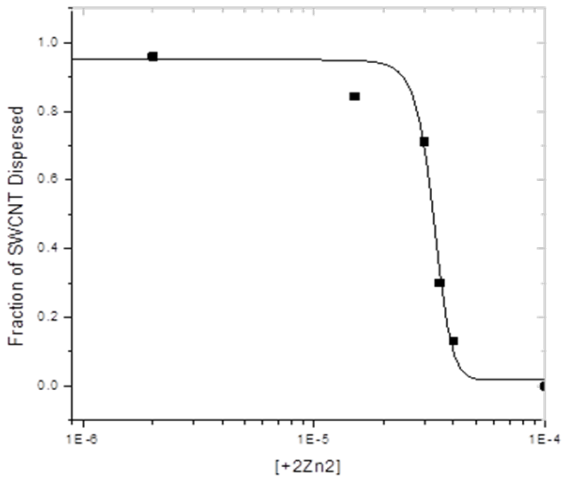

Figure 3.1.3: Dispersion stability curve for SG 6,5 SWCNTs with +2Zn2. The Boltzmann sigmoidal function was used to calculate the dispersion stability to be 32.9 ± 0.4 μM. X axis represents the concentration of the spacer and Y axis represents the fraction dispersed from the tubes, which is the final concentration normalized to the control.

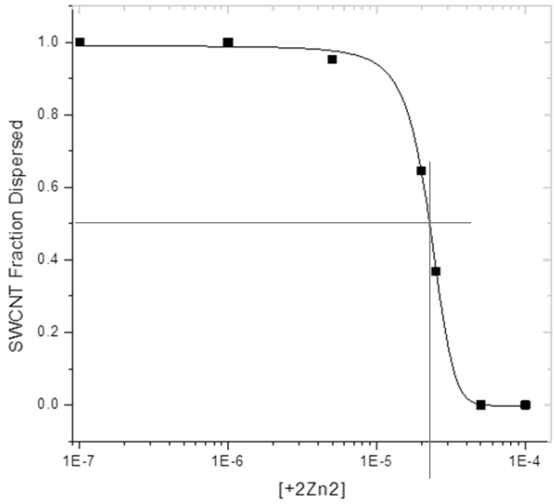

Figure 3.1.4: Dispersion stability curve for SG 7,6 SWCNTs with +2Zn2. The Boltzmann sigmoidal fuction was used to calculate the dispersion stability to be 22.7 ± 0.3 µM. X axis represents the concentration of the spacer and Y axis represents the fraction dispersed from the tubes, which is the final concentration normalized to the control.

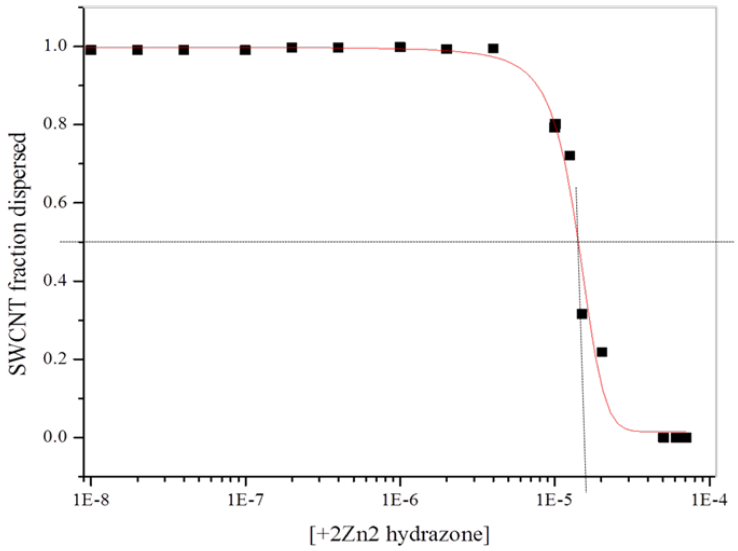

Figure 3.1.5: Dispersion stability curve for HiPco SWCNTs with +2Zn2. The Boltzmann sigmoidal function was used to calculate the dispersion stability to be 14.2 ± 0.3 µM. X axis represents the concentration of the spacer and Y axis represents the fraction dispersed from the tubes, which is the final concentration normalized to the control.

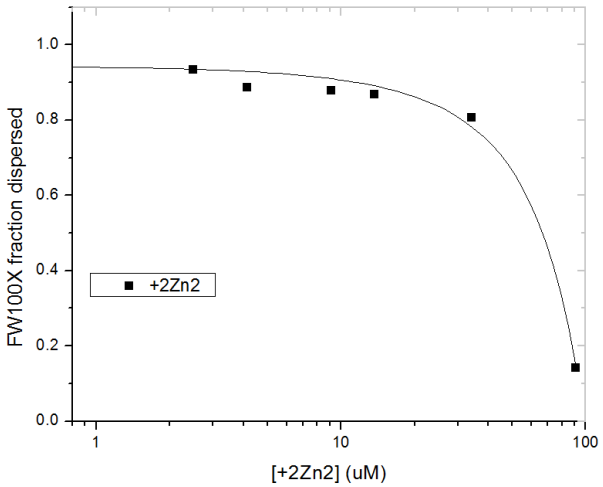

Figure 3.1.6: Dispersion stability curve for FWCNTs with +2Zn2. The Boltzmann sigmoidal function was used to calculate the dispersion stability to be 35 ± 6 µM. X axis represents the

concentration of the spacer and Y axis represents the fraction dispersed from the tubes, which is the final concentration normalized to the control.

CNTs	**Diameter (nm)**	**X_0 (μM)**
SG 6,5	0.75	1.37 ± 0.02
HiPco	0.95	1.35 ± 0.02

Table 3.1.2: Dispersion stabilities of CNTs in +2Ru2 coordination complex with their corresponding tube diameters.

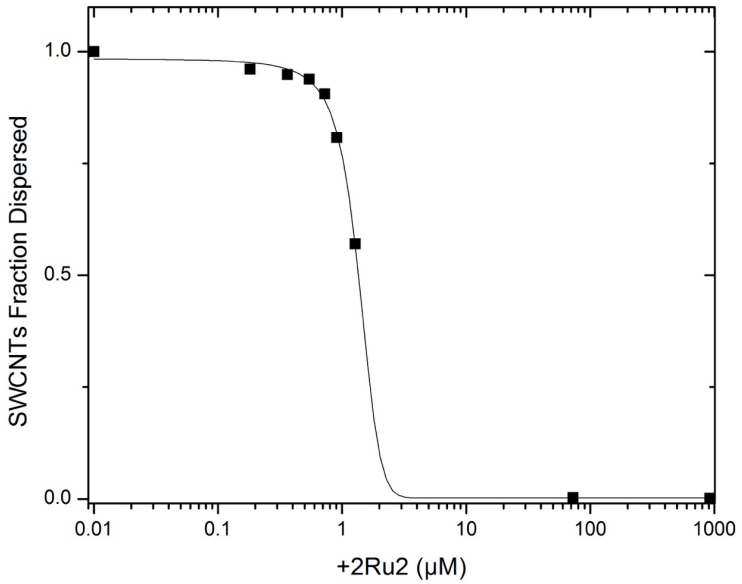

Figure 3.1.7: Dispersion stability curve for HiPco SWCNTs with +2Ru2. The Boltzmann sigmoidal function was used to calculate the dispersion stability to be 1.37 ± 0.02 μM. X axis represents the concentration of the spacer and Y axis represents the fraction dispersed from the tubes, which is the final concentration normalized to the control.

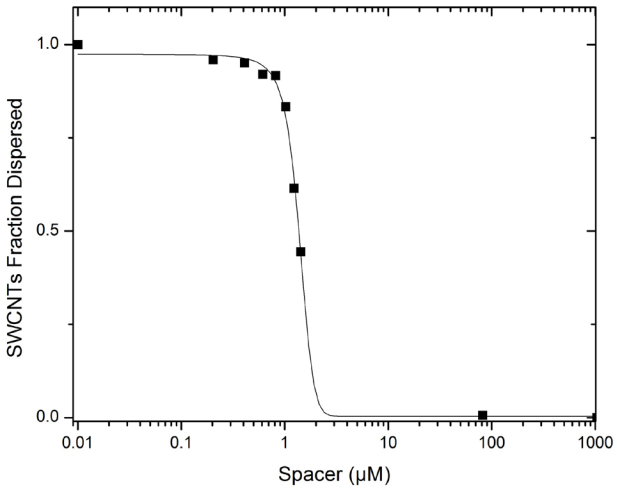

Figure 3.1.8: Dispersion stability curve for SG 6,5 SWCNTs with +2Ru2. The Boltzmann sigmoidal function was used to calculate the dispersion stability to be 1.35 ± 0.02 μM. X axis represents the concentration of the spacer and Y axis represents the fraction dispersed from the tubes, which is the final concentration normalized to the control.

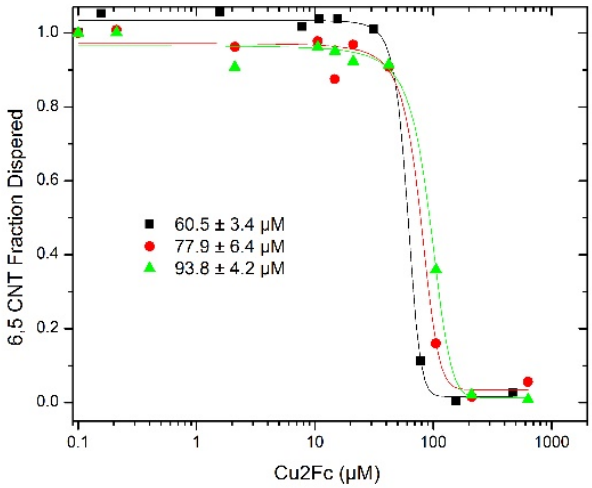

Figure 3.1.9: Dispersion stability curve for SG 6,5 SWCNTs with Cu2FcOH. The Boltzmann sigmoidal function was used to calculate the dispersion stability to be 77.4 ± 2.8 μM. X axis represents the concentration of the spacer and Y axis represents the fraction dispersed from the tubes, which is the final concentration normalized to the control.

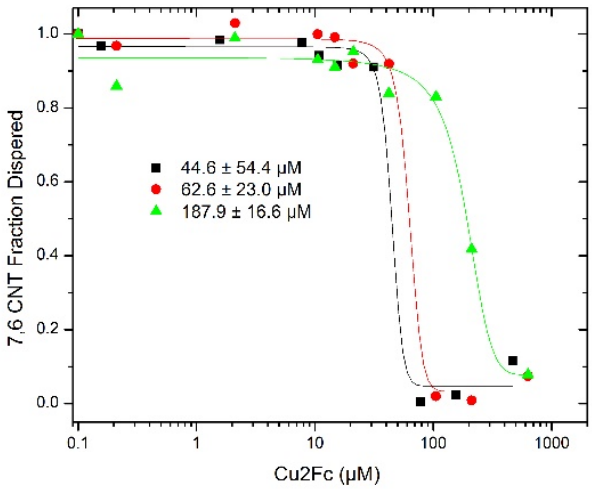

Figure 3.1.10: Dispersion stability curve for SG 7,6 SWCNTs with Cu2FcOH. The Boltzmann sigmoidal function was used to calculate the dispersion stability to be 98 ± 20 μM. X axis represents the concentration of the spacer and Y axis represents the fraction dispersed from the

tubes, which is the final concentration normalized to the control.

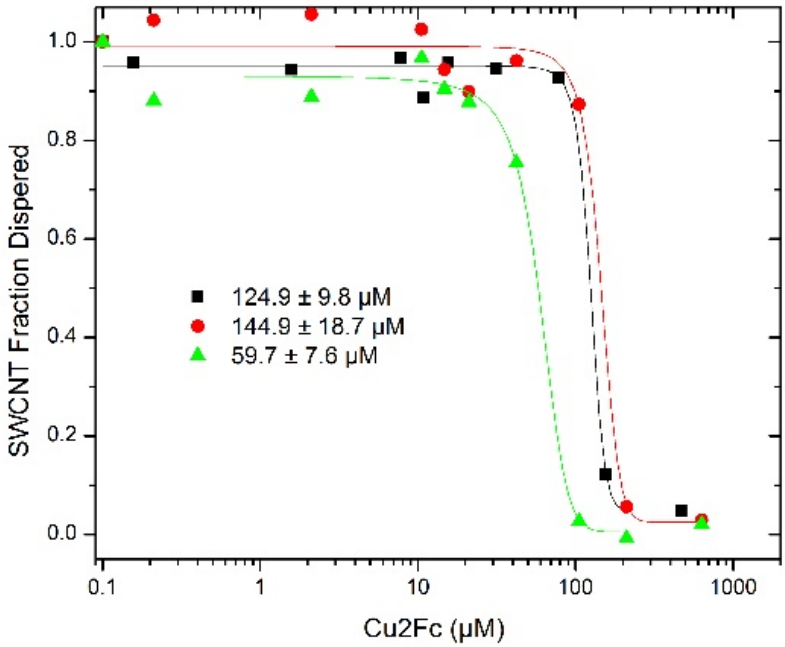

Figure 3.1.11: Dispersion stability curve for HiPco SWCNTs with Cu2FcOH. The Boltzmann sigmoidal function was used to calculate the dispersion stability to be 110 ± 7 μM. X axis represents the concentration of the spacer and Y axis represents the fraction dispersed from the tubes, which is the final concentration normalized to the control.

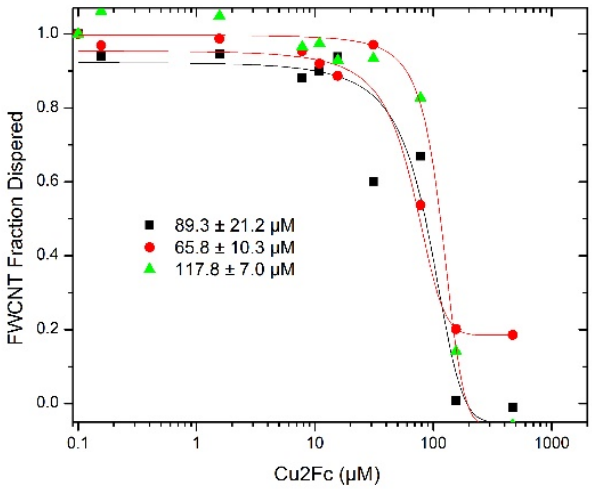

Figure 3.1.12: Dispersion stability curve for FWCNTs with Cu2FcOH. The Boltzmann sigmoidal function was used to calculate the dispersion stability to be 91 ± 8 μM. X axis

represents the concentration of the spacer and Y axis represents the fraction dispersed from the tubes, which is the final concentration normalized to the control.

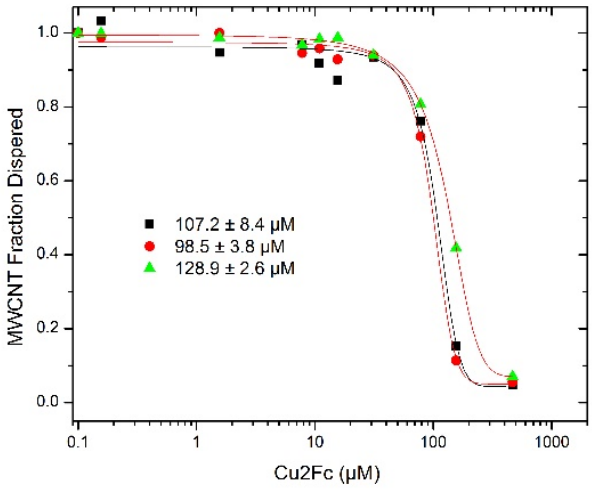

Figure 3.1.13: Dispersion stability curve for MWCNTs with Cu2FcOH. The Boltzmann sigmoidal function was used to calculate the dispersion stability to be 111 ± 3 μM. X axis represents the concentration of the spacer and Y axis represents the fraction dispersed from the tubes, which is the final concentration normalized to the control

CNTs	**Diameter (nm)**	**X_0 (μM)**
SG 6,5	0.75	77.4 ± 2.8
SG 7,6	0.88	98 ± 20
HiPco	0.95	110 ± 7
FW100X	2.03	91 ± 8
MWCNT	8.0	111 ± 3

Table 3.1.3: Dispersion stabilities of CNTs in Cu2FcOH coordination complex with their corresponding tube diameters.

Spacers	**+2Zn2**	**Cu2FcOH**
Dis. Stability **X_0 (μM)** (HiPco)	40.5 ± 0.4	110 ± 7

Table 3.1.4: Dispersion stabilities of HiPco SWCNTs in +2Zn2 and Cu2FcOH coordination complexes.

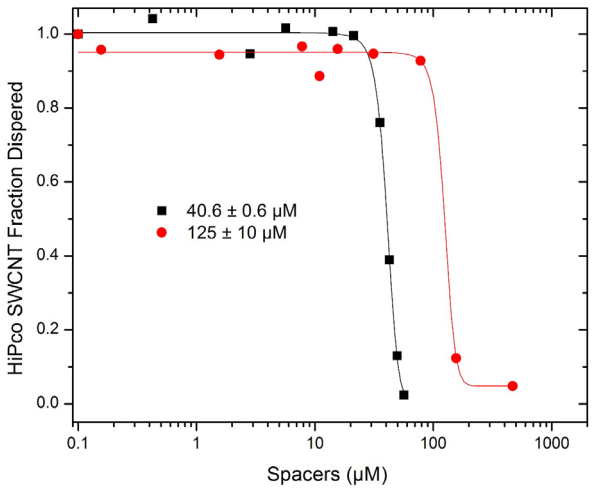

Figure 3.1.14: Dispersion stability curve for HiPco SWCNTs with +2Zn2 (black) and Cu2FcOH (red). The Boltzmann sigmoidal function was used to calculate the dispersion stability to be 40.5 ± 0.4 and 110 ± 7 μM respectively. X axis represents the concentration of the spacer and Y axis represents the fraction dispersed from the tubes, which is the final concentration normalized to the control.

Spacers	**+2Zn2**	**+2Ru2**
Dis. Stability **X_0 (μM)**(HiPco)	40.5 ± 0.4	1.36 ± 0.02

Table 3.1.5: Dispersion stabilities of HiPco SWCNTs in +2Zn2 and +2Ru2 coordination complexes.

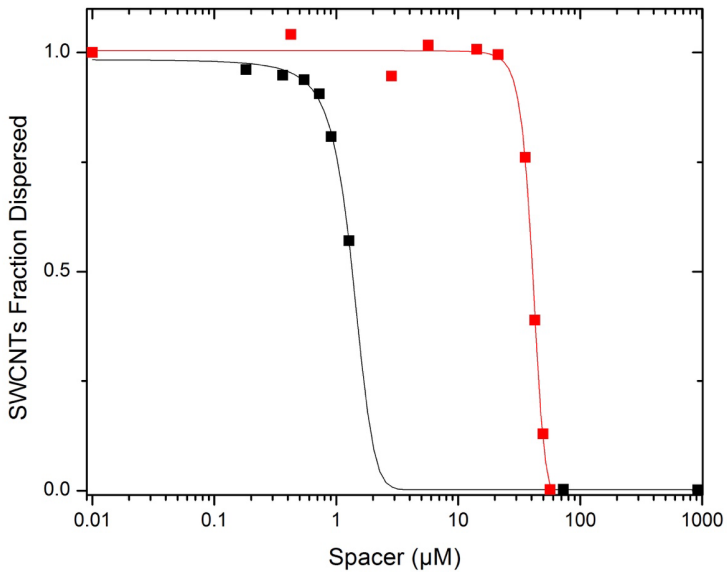

Figure 3.1.15: Dispersion stability curve for HiPco SWCNTs with +2Ru2 (black) and +2Zn2 (red). The Boltzmann sigmoidal function was used to calculate the dispersion stability to be = 1.36 ± 0.02 and 40.5 ± 0.4 μM respectively. X axis represents the concentration of the spacer and Y axis represents the fraction dispersed from the tubes, which is the final concentration normalized to the control.

3.2 Adsorption Studies

Adsorption of molecular spacers can be illustrated through LRI such as electrostatic interactions, Van der Waals and π-π stacking. The positive charge on the surface of the molecular coordination complexes leads to higher binding with CNTs that have partial negative charge due to π electrons and also the presence of conjugated rings and ferrocene ligands leads to higher π-π stacking with the carbon rings of the tubes. The amount of spacer bound to CNTs is the q_e which is the mg of coagulant (adsorbate) per g of SWCNTs adsorbent.

Brunsauer-Emmett-Teller (BET) model is used to analyze the adsorption isotherm as shown below:

$$q_e = q_m \frac{K_s C_{eq}}{(1-K_L C_{eq})(1-K_L C_{eq}+K_s C_{eq})}$$

Where q_e represents equilibrium bound adsorbate. q_m is the adsorbate loading of one monolayer. K_s is a constant of surface interaction of the spacer with CNTs. K_L represents subsequent adsorb layer bound to the first monolayer and C_{eq} is the equilibrium concentration of the spacer . +2Zn2 adsorption isotherm was previously conduced to HiPco tubes and SG 6,5 at two concentrations 5.3 mg L^{-1} and 10.9 mg L^{-1} . The adsorption isotherms were analyzed by Brunauer-Emmett-Teller (BET) model. It was observed that HiPco tubes show higher binding capacity than SG 6,5 and this can be observed too from the dispersion stability results since SG 6,5 has a higher stability than the HiPco due to less interaction with the coagulant.

Spacers	**SG 6,5**	**HiPco**
q_e (mg coagulant/g SWCNT)	616	790

Table 3.2.1: The amount of spacer bound to HiPco SG 6,5 SWCNTs .

It was hypothesized that +2Zn2 binds more strongly to the larger tubes because there is less strain on the complex to bind around the surface of the tube, i. e., +2Zn2 binds more strongly to the larger HiPco (7,7) tubes causing the EDL to collapse and that forces the system to aggregate, which drastically reduces the SSA, making the tubes less effective in energy storage application. Smaller tubes have higher dispersion stability than larger ones, but FWCNTs had a high dispersion stability and it is not currently understood why, but an explanation was proposed that it is either the zeta potential of the tubes is high, which means FWCNTs has high degree of

electrostatic repulsion between similar charged particles, or that for some unknown reason, these tubes do not bind strongly to the coagulant and that can be studied by conducting adsorption isotherm measurements. To finish the CNTs comparison, +2Zn2 adsorption isotherm was conducted to FWCNT to investigate the proposed hypothesis that FWCNT should have lower dispersion stability.

Due to the difficulty in dispersing the FWCNTs in DMF, their adsorption isotherm were hard to obtain. However, the obtained Ks value was reproducible. The BET model was used to analyze the data. HiPco tubes have a higher q_e than SG 6,5 (Fig. 3.2.1), but for FWCNTs, the data were not stable and showed a low K_s value, which represents the binding strength of the tubes to the spacer +2Zn2 and that explains the high dispersion stability previously obtained. (Table 3.1.1). Adsorption isotherm measurements of +2Cu2FcOH with SG 6,5 tubes (Fig 3.2.2) showed shallow slope indicating low binding with the tubes While the adsorption isotherm measurements of +2Ru2 with SG 6,5 tubes (Fig 3.2.3) showed higher binding with steeper slope. However, one of the points showed a point where q drops (Fig 3.2.3) indicating some issues with the experiment that needs further investigation to be solved.

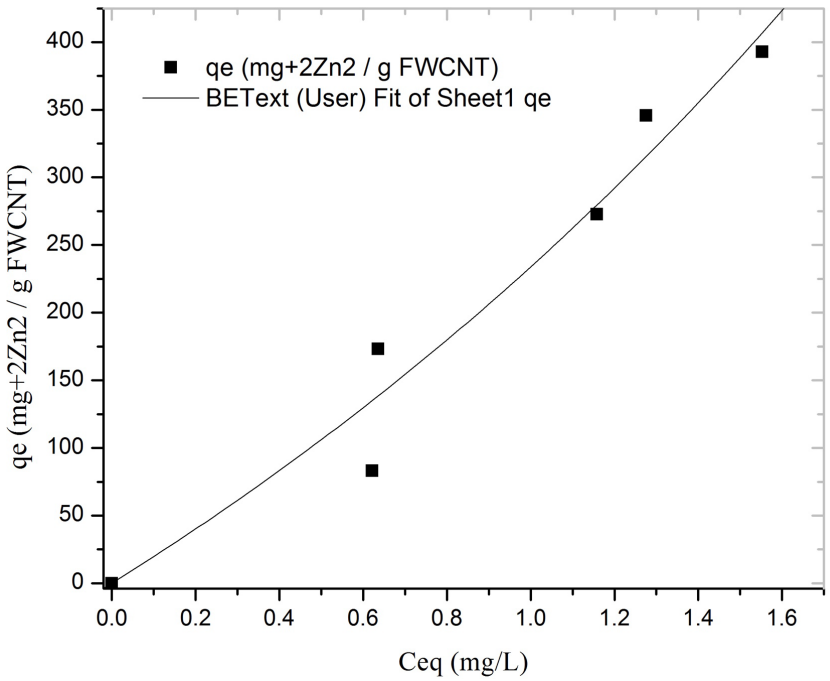

Figure 3.2.1: +2Zn2 adsorption isotherm modeled based on BET theory (FWCNTs). X axis represents the equilibrium concentration of the spacer and Y axis represents the mass of the adsorbate over the adsorbent.

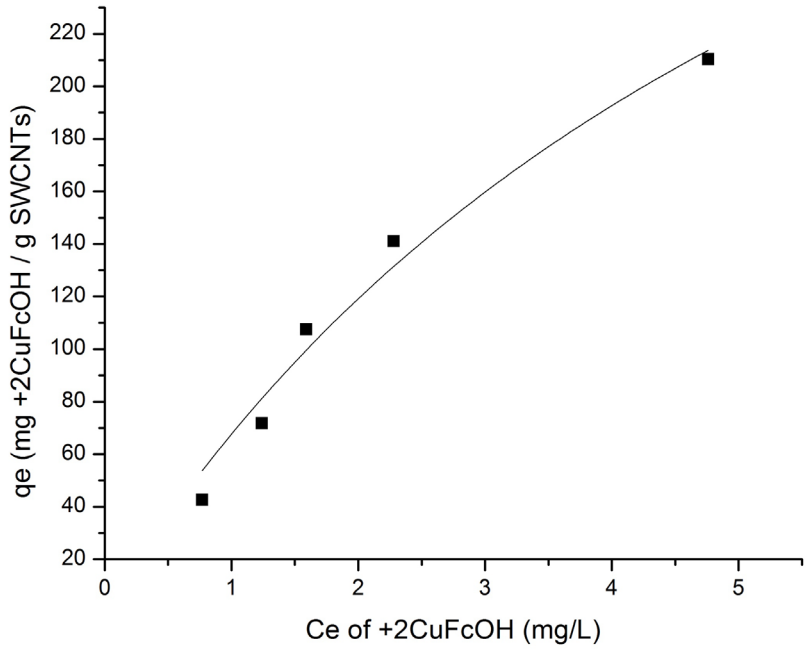

Figure 3.2.2: +2Cu2FcOH adsorption isotherm data of SG 6,5. X axis represents the equilibrium concentration of the spacer and Y axis represents the mass of the adsorbate over the adsorbent.

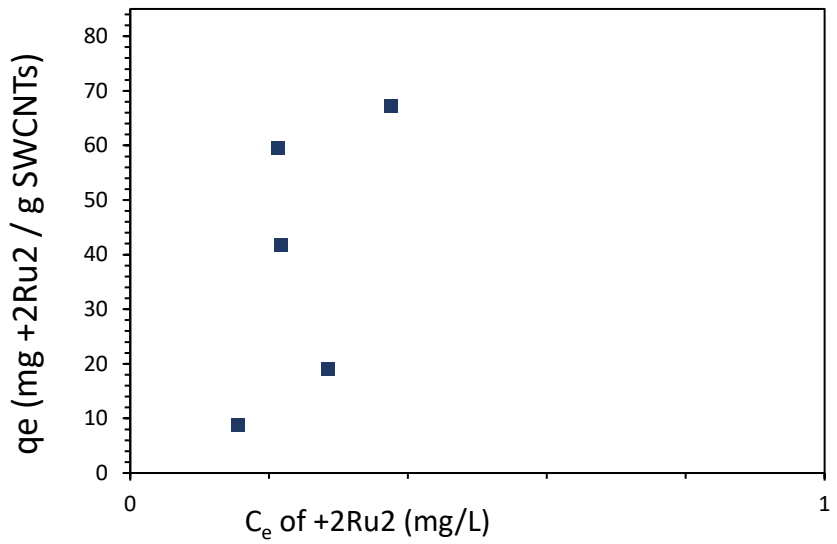

Figure 3.2.3: +2Ru2 adsorption isotherm data of SG 6,5. X axis represents the equilibrium concentration of the spacer and Y axis represents the mass of the adsorbate over the adsorbent.

3.3 Zeta Potential and Size Measurements

To test the proposed hypothesis that the high stability of FWCNTs might be due to its high zeta potential, zeta potential adsorption isotherm measurements were conducted. Zeta potential data showed that there is not huge difference between the zeta potential of FWCNTs compared to the other which negates the first hypothesized reason for the high obtained dispersion stability of the tubes. However, adsorption isotherm measurements gave small k_s values which represents the binding strength of CNTs to the spacer and that means that +2Zn2 does not bind to FWCNTs with same strength as it binds to the other tubes, making them having a higher dispersion stability.

CNTs	Diameter (nm)	Zeta Potential (mV)
SG 6,5	0.75	-28 ± 6
SG 7,6	0.88	-43 ± 11
HiPco	0.95	-51 ± 11
FW100X	2.03	-32 ± 6

Table 3.3.1: Zeta Potential of four CNTs of interest in DMF solvent with their corresponding tube diameters.

3.4 UV-Vis NIR Spectroscopy

UV-Vis spectroscopy is an important analytical technique to identify variant analytes such as coordination metals and conjugated systems. A fundamental understanding of how excited electrons move throughout the coordination complexes can be understood though using the absorption of light of our spacers. In Fig. 3.5.1, absorption of **+2Ru2** around 441 (ε = 225000 M^{-1} cm^{-1}) is attributed to metal to ligand charge transfer, and 375 nm (ε = 257600 M^{-1} cm^{-1}) are consistent with π to π^* transitions [9]. In Fig. 3.5.4, absorptions of **+2Zn2** around 425 (ε = 22960 M^{-1} cm^{-1}) and 470 nm (ε = 15720 M^{-1} cm^{-1}) are consistent with ion-pair to π^* charger transfer transitions, while the absorption around 320 nm (ε = 8580 M^{-1} cm^{-1}) is most likely π to π^* transitions based on preliminary density functional theory (DFT) calculations.[8] The **Cu2FcOH** and **+2Cu2FcOH** coordination complexes have two ferrocene moieties which absorb light around 415 nm (ε = 10290 M^{-1} cm^{-1}). Less delocalization of electrons in the ferrocene moieties are a possible explanation of the shifting absorption of ferrocene typically seen around 450 nm.[11]

UV absorptions around 330 nm (ε = 17600 M^{-1} cm^{-1}) are also consistent with π to π^* electron transfer.[11] These strong absorption bands show charge transfer through the molecular spacers. By intercalating the molecular spacers between CNTs, ion-transport is anticipated to further increase compared to pristine CNTs because of increased ion-accessible SSA and an electronically conductive bridge between nanotubes.

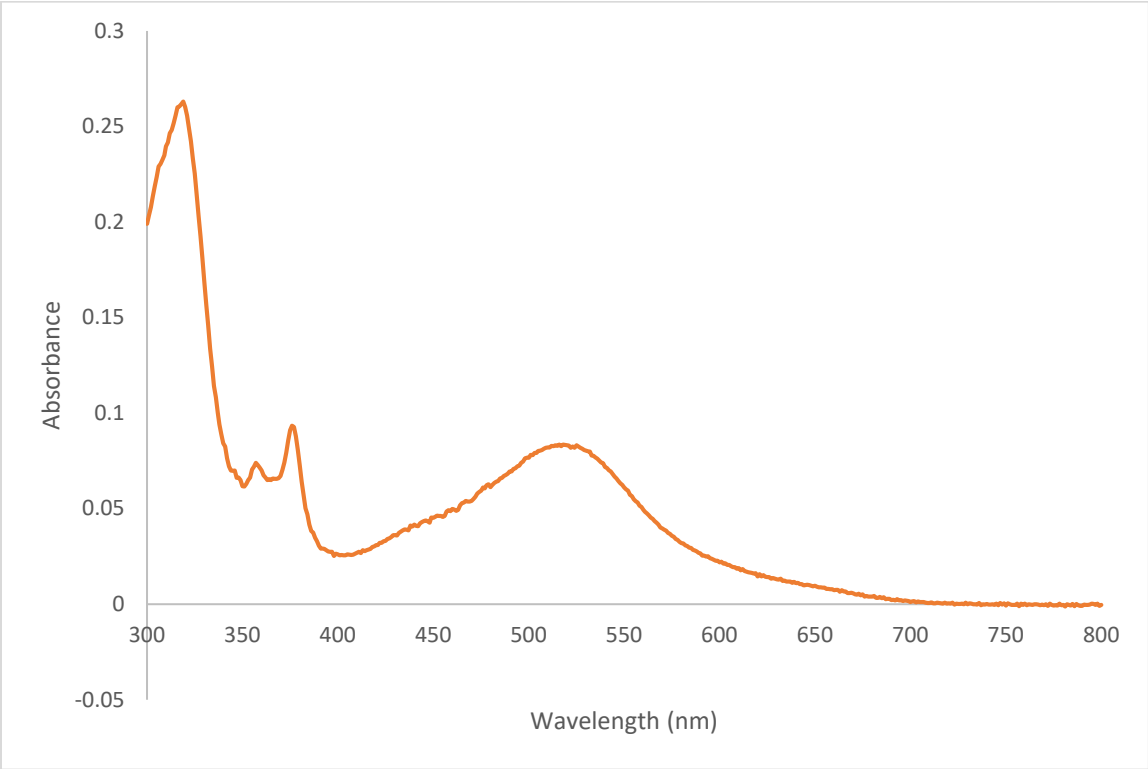

Figure 3.5.1: UV-Vis spectrum of +2Ru2 coordination compex.

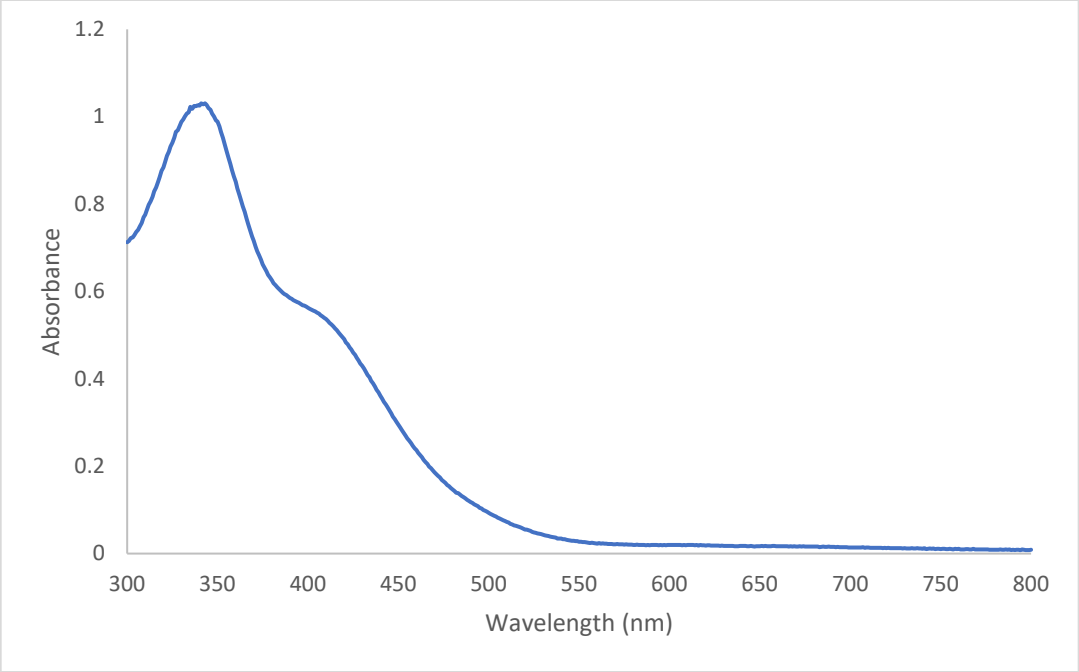

Figure 3.5.2: UV-Vis spectrum of +2Cu2FcOH coordination compex.

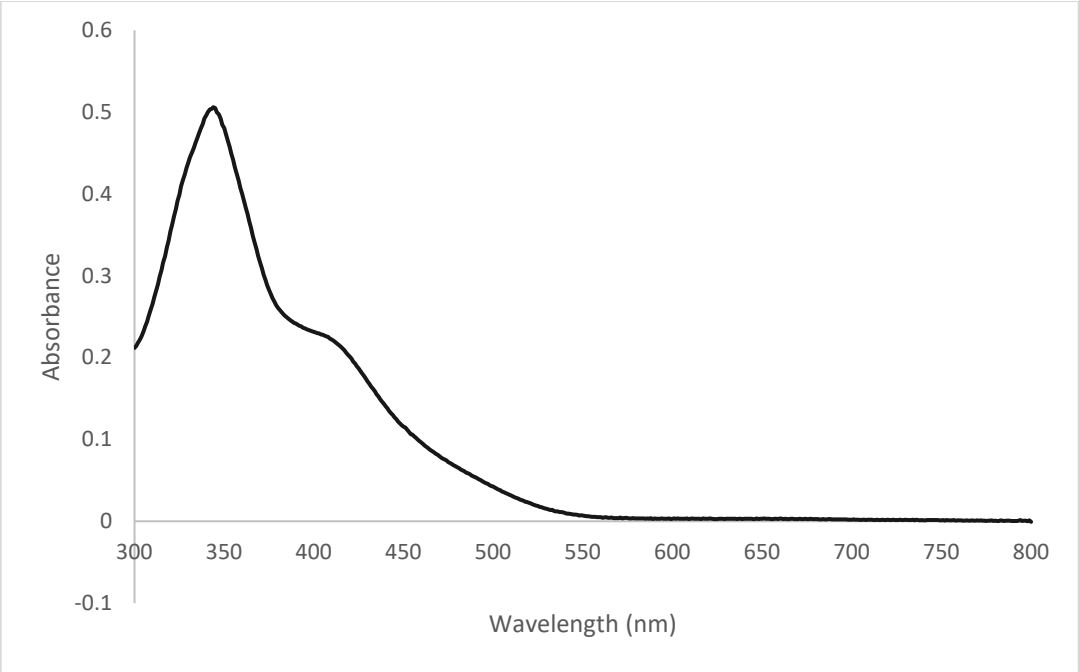

Figure 3.5.3: UV-Vis spectrum of Cu2FcOH coordination compex.

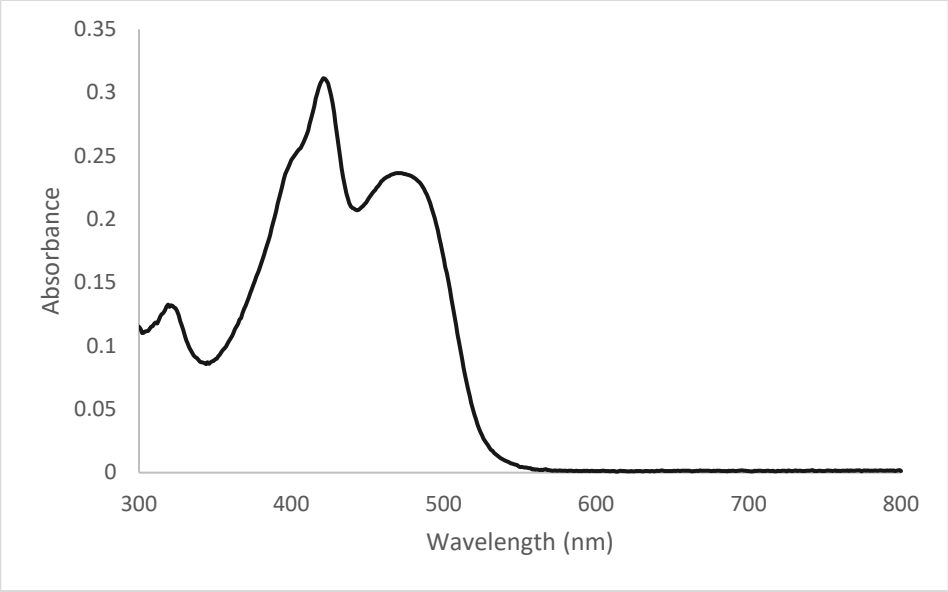

Figure 3.5.4: UV-Vis spectrum of +2Zn2 coordination compex.

3.5 Membrane Resistance Measurements

Having the molecular spacer intercalated between the tubes works as a barrier preventing the repulsion between the tubes decreasing their aggregation. Having those molecular barrier should increase the porosity of the tubes and therefore decrease membrane resistance (MR). Membrane resistance measurements have been conducted to pristine SWCNTs and to spacer-SWCNTs dispersion in order to test the efficiency of the spacer separation of the tubes. According to the hypothesis, adding the molecular spacer should increase SSA and therefore the flow rate through spacer-SWCNTs thin films. The MR of the pristine CNTs film is expected to be higher than that of the spacer-SWCNTs films. The flux Q of DMF through SWCNTs and spacer-SWCNTs thin films was measured and MR have been determined using Darcy's Law

$$K_m = \frac{\alpha \Delta P}{\mu Q}$$

where ΔP is the difference of pressure across the membrane, μ is the dynamic viscosity and α is the area of the film. The MR of equivalent pristine films gave different numbers (Fig. 3.5.1) which was not expected and still needs further research or better measurement technique to solve. It was hypothesized that amount of the DMF in the films might be the cause of this inconsistency in the MR measurements. Therefore, the MR was measured for equivalent pristine films that have been dried for different time periods. The MR of the pristine films dried for different periods showed the same inconsistency even after the drying, and that proves that the MR of the tube is independent of the amount of DMF on the membrane (Fig. 3.5.2). However, when the MR was measured to compare the porosity of pristine and spacer-SWCNTs films, the MR of spacer-SWCNTs films was lower than the MR of the pristine CNTs and kept increase with increasing DMF rinses. The result agrees with the proposed hypothesis proving that the presence of spacer prevent the aggregation of the tubes, increase the SSA, and eventually will lead to higher increase storage and therefore higher capacitance (Fig. 3.5.3).

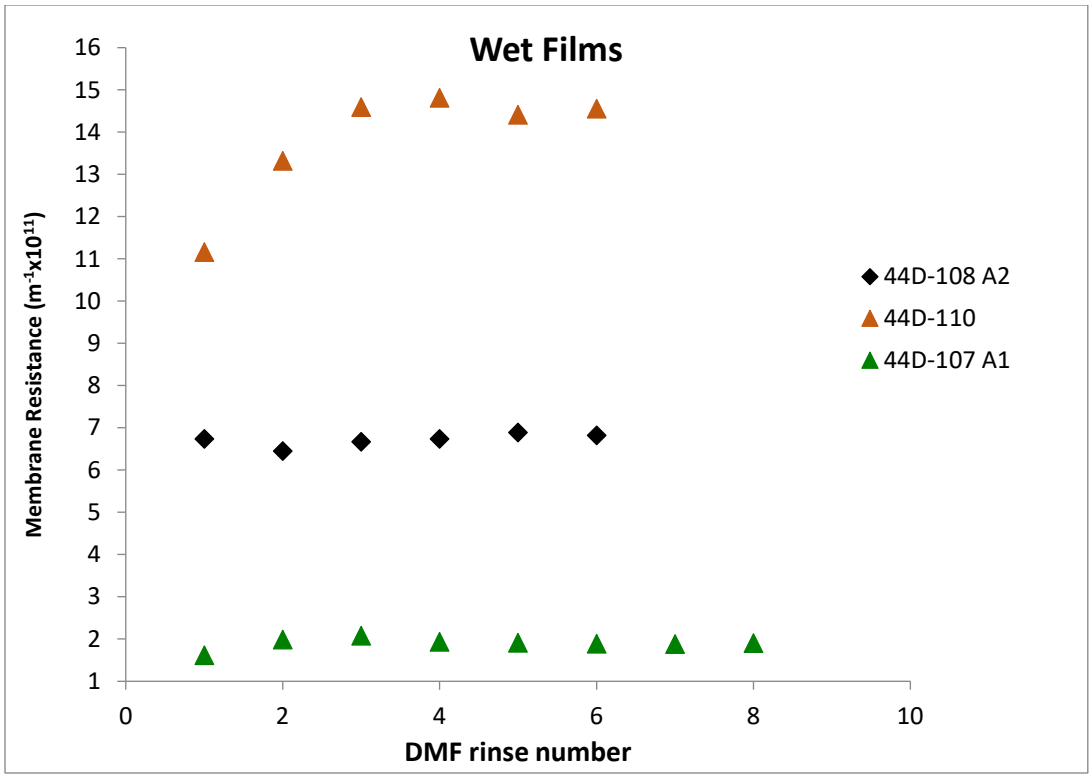

Figure 3.5.1: membrane resistance "Successive DMF Rinses method" wet films. Obs. Although these samples were made in nearly the same conditions, they still show different membrane resistance values.

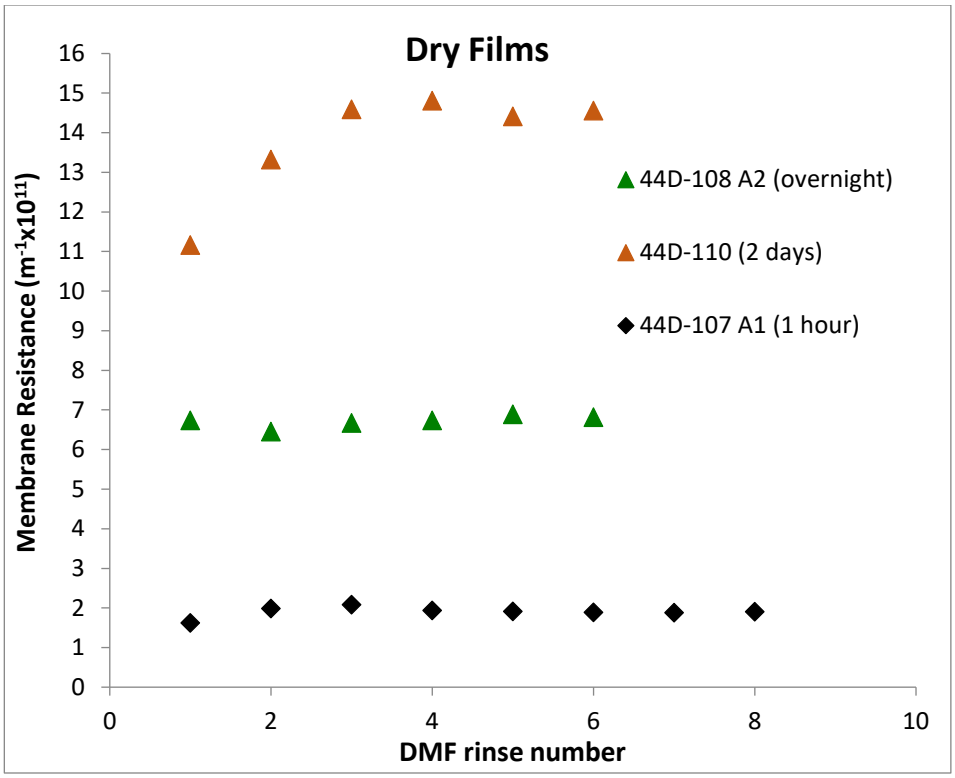

Figure 3.5.2: membrane resistance "Successive DMF Rinses method" vacuum dried films. Obs. The one that dried most (for two days), which supposed to have the lowest amount of DMF, had the highest resistance**.** We can observe that the amount of the DMF in the film does not affect its permeability.

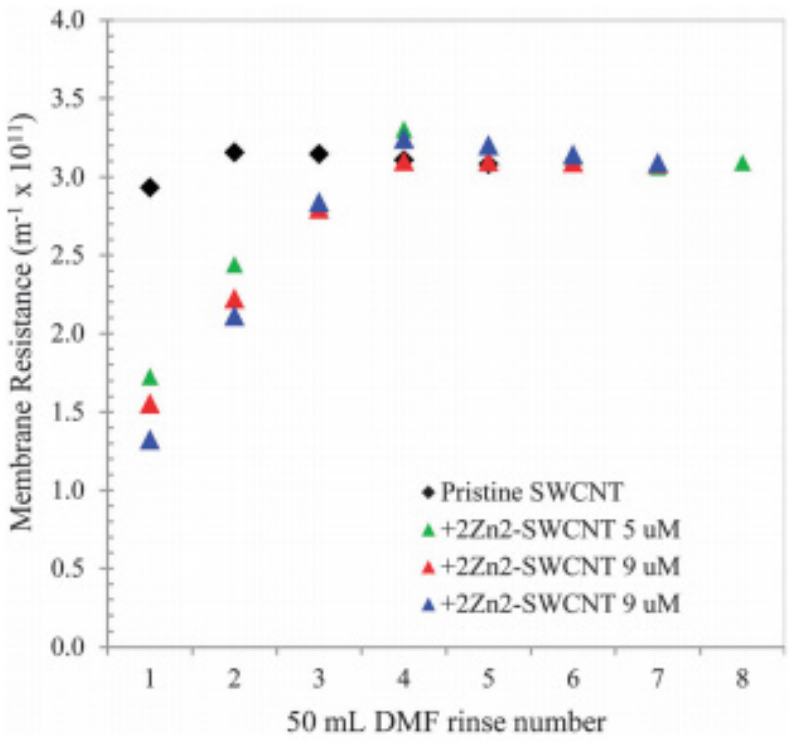

Figure 3.5.3: membrane resistance **"**Successive DMF Rinses method". Obs. The MR of the spacer-SWCNTs thin films increases with increase the number of DMF Rinses. The spacer-SWCNTs films showed lower MR than the pristine films (diamond)[8]

CHAPTER 4: CONCLUSIONS AND FUTURE WORK

We have studied single-walled carbon nanotubes (SWCNTs) for use as potential supercapacitor materials. Central to these applications are studies of the dispersion limit of SWCNTs in different solvents, and how various dinuclear coordination complexes interact with them. These complexes have high adsorption onto SWCNTs' surfaces and act as a "Molecular Spacer", which results in less aggregation. Keeping the nanomaterials from aggregating is required to maximize the ion accessible surface area (SSA). When the stability of SWCNTs-Molecular spacer assembly is enhanced, the capacity of the system improves. Binding kinetics and adsorption studies of novel earth-abundant coordination complexes were conducted. Molecular spacers intercalated between the tubes that increased ion accessible surface area. Different molecular spacers with various charges and steric interactions were tested and compared. Dispersion stability and aggregation kinetics were conducted using different pristine SWCNTs and with different coagulants adsorbed onto their surfaces. Carbon nanotubes showed high stability with +2Zn2 as the size decreases and that is consistent with the hypothesis that the spacer binds more strongly to the larger tubes collapsing the electrical double layer and leading to an aggregation. However, FWCNTs showed the highest dispersion stability among all of the tubes, which contradicts the proposed hypothesis; therefore, an explanation was proposed that either FWCNTs have a high zeta potential, which means FWCNTs have a high degree of electrostatic repulsion between similar charged particles, or that, for some unknown reason, these tubes do not bind strongly to the coagulant. FWCNTs had zeta potential value that was very close to these of other tubes which invalidated hypothesis invalid. Then, FWCNTs was studied by conducting adsorption isotherm measurements and the results showed low binding strength and that explains its high observed dispersion stability. Carbon nanotubes showed higher stability with Cu2FcOH

as the size increases and that might be attributed due to lack of charge on the spacer which increase the binding with the larger tubes and speed their aggregation. Due to the low stability of CNTs in +2Ru2 coordination complex, the stability did not show significant difference as the tube diameter changes. Further research is needed to investigate the inconsistency in adsorption isotherm data with the spacer. A better technique might be required in order to get a reproducible data whenever the measurements is conducted. By using Earth abundant molecular spacers, we aim to increase ion accessible surface area of SWCNT for energy storage devices. Current battery technologies can store high amounts of energy, but their high cost, low charge/discharge rates, and short lifetime make them impractical in grid-scale systems. By increasing capacitance and preventing aggregation from molecular spacers, we hope to be able to use thin films as electrodes in supercapacitors.

BIBLIOGRAPHY

1. R. E. Sims, H. H. Rogner, K. Gregory, *Energy policy*, 2003, 31.13, 1315-1326.

2. U.S. Energy Information Administration, *Monthly Energy Review*, https://www.eia.gov/totalenergy/data/monthly/previous.php#2016, (accessed April 2018).

3. A Nishino, A Yoshida, I Tanahashi, *US Pat.,* 1985, 4, 562, 511.

4. Defense Logistics Agency, *DLA: The Right Solution – On Time, Every Time.* http://www.mpoweruk.com/performance.htm, (accessed April 2018).
5. Y. Yang, T. Liu, L. Zhang, S. Zhao, W. Zeng, S. Hussain. C. Deng. H. Pan, X. Peng, *J Mater Sci:Mater Electron,* 2016, 27, 6202–6207.
6. Q. Wang, Z. Wen, J. Li, *Adv. Funct. Mater*, 2006, 16, 2141-2146.
7. Y. Xie, X. Fang, *Electrochimica Acta*, 2014, 120, 273-283.
8. A. A. Ameen, A. N. Giordano, J. R. Alston, M. W. Forney, N. P. Herring, S. Kobayashi, S. G. Ridlen, S. S. Subaran, T. J. Younts and J. C. Poler*, *Phys. Chem. Chem. Phys.,* 2014, 16 (12), 5855 – 5865.
9. J. R. Alston, D. J. Banks, C. X. McNeill, J. B. Mitchell, L. D. Popov, I. N. Shcherbakov, and J. C. Poler*, *Phys. Chem. Chem. Phys,* 2015, 17, 29566 – 29573.
10. M. W. Forney, J. C. Poler, *J. Phys. Chem. C* 2011, 115 (21), 10531-10536.
11. L. D. Popov, I. N. Shcherbakov, S. I. Levchenkov, Y. P. Tupolova, V. A. Kogan and V. V. Lukov, Binuclear copper(II) and oxovanadium(IV) complexes with 2,6-diformyl-4-tert-butylphenol-bis-(10-phthalazinylhydrazone). Synthesis, properties and quantum chemical study *Journal of Coordination Chemistry*, **2008**, 61, 392-409.

12. S. I. Levchenkov, E. A. Raspopova, A. N. Morozov, L. D. Popov, Y. V. Titova, M. O. Gorbunova and I. N. Shcherbakov, 2,6-diformyl-4-tert-butylphenol bis-ferrocenoylhydrazone and binuclear copper(II) complexes on its basis *Russian Journal of General Chemistry*, **2016**, 86, 2075-2080.
13. R. Trivedi, S. B. Deepthi, G. Lingamallu and K. V. S. Ramakrishna, Synthesis, Crystal Structure, Electronic Spectroscopy, Electrochemistry and Biological Studies of Ferrocene-Carbohydrate Conjugates *EurJIC*, **2012**, 2012, 2267-2277.